Energetic Requirements for Dynamos in the Metallic Cores of Super-Earth Exoplanets

C. H. Blaske[1,2], J. G. O'Rourke[2]

[1]Barrett, The Honors College, Arizona State University, Tempe AZ

[2]School of Earth and Space Exploration, Arizona State University, Tempe AZ

Corresponding author: J. G. O'Rourke (jgorourk@asu.edu)

Key Points:

- Super-Earths are massive exoplanets with Earth-like bulk compositions but surface conditions that could be Earth- or Venus-like
- We calculated how fast their metallic cores must cool to sustain a dynamo powered by thermal or chemical convection
- Massive Earth- and Venus-analogues may both host dynamos and potentially detectable magnetospheres if their silicate mantles are solid

Abstract

Super-Earths are massive exoplanets with Earth- and Venus-like bulk compositions and surfaces of questionable habitability. Vigorous convection within their metallic cores may produce strong magnetospheres if the total heat flow out of the core exceeds a critical value. Earth has a core-hosted dynamo because plate tectonics cools the core relatively rapidly. In contrast, Venus has no dynamo and its deep interior probably cools slowly. However, studies of super-Earths have reached disparate conclusions about the prospects for core-hosted dynamos. Here we develop scaling laws for how planetary mass affects the minimum heat flow required to sustain both thermal and chemical convection, which we compare to a simple model for the actual heat flow conveyed by solid-state mantle convection. We found that the required heat flows increase with planetary mass (to a power of ~0.9), but the actual heat flow may increase even faster (to a power of ~1.7). Massive super-Earths are likely to host a dynamo in their metallic cores if their silicate mantles are entirely solid. Super-Earths with Venus-like geodynamics could host a dynamo if their mass exceeds ~1.4 (chemical convection) or ~3 (thermal convection) Earth-masses. Crucially, the silicate mantles of super-Earths might not be completely solid. Basal magma oceans may reduce the heat flow across the core-mantle boundary and smother any core-hosted dynamo. Detecting a magnetosphere at an Earth-mass planet probably signals Earth-like geodynamics. In contrast, magnetic fields may not reliably probe whether a super-Earth is a true Earth-analogue. We eagerly await direct observations in the next few decades.

Plain Language Summary

Earth is the largest planet in our Solar System chiefly composed of silicates and metal. However, we now know that so-called Super-Earths—made of rock and metal in Earth-like proportions but with larger masses—are common in our galaxy. No one knows if their surfaces are habitable like Earth or hellish like Venus. Earth's magnetosphere, which has survived for billions of years, is perhaps a symptom of habitability. Without our liquid water oceans and mild temperatures, Earth might not have plate tectonics, which cools Earth's rocky mantle and metallic core relatively quickly. In contrast, Venus may lack a dynamo because its core cools slowly. Detecting any magnetic field from super-Earths may become possible in a few decades. Would such a detection reveal a true Earth-analogue? Here we calculate the minimum heat flow out of massive metallic cores required to sustain a dynamo under different circumstances. We compare these minimums

to a simple model of the actual heat flow. We find that a super-Earth without a magnetic field is probably not a scaled-up Earth. However, massive Venus-analogues with inner cores may also host magnetic fields. Ultimately, more studies are required to constrain the factors that can help or hinder dynamos in terrestrial planets.

1 Introduction

Thousands of exoplanets have been discovered since the Kepler Space Telescope was launched in 2009, and the pace of discovery is only increasing. So-called super-Earths are common in our galaxy but have no known analogue in our Solar System. Colloquially, a super-Earth is an exoplanet with an Earth-like (i.e., rock/metal) composition and a mass between 1 and 10 Earth-masses. It cannot be overemphasized that super-Earths need not have Earth-like surface conditions (e.g., Tasker et al., 2017). Venus has the same bulk composition as Earth but its surface is a hellish wasteland (e.g., Kane et al., 2019). No super-Earth exoplanet is yet distinguishable from a super-Venus (e.g., Foley et al., 2012; Foley & Driscoll, 2016; Kane et al., 2014). Observationally, planets with radii larger than ~1.5 Earth-radii (~5 Earth-masses) mostly have low densities, implying that they acquired thick, volatile envelopes and are perhaps "mini-Neptunes" (e.g., Rogers, 2015; Weiss & Marcy, 2014). Extremely massive super-Earths may still exist in our galaxy even if they are statistically rare. Super-Earths are intrinsically interesting—and they provide a unique opportunity to study how planetary mass affects planetary evolution.

Magnetic fields may open unique windows into the internal structure and dynamics of super-Earths. In general, planetary magnetospheres may shield the surface from the solar wind (e.g., Driscoll, 2018) and can affect atmospheric loss processes over time (e.g., Dong et al., 2020). Terrestrial planetary bodies in our Solar System (e.g., Mercury, Venus, Earth, Earth's Moon, and Mars) are differentiated into silicate mantles and metallic cores. All of these bodies, possibly excepting Venus, have global magnetic fields produced by dynamos in their metallic cores now or had such fields in the past (e.g., Stevenson, 2003, 2010). Ultimately, vigorous convection in metallic cores—driven by the loss of heat to the silicate mantle—produces dynamos. Our Solar System provides too small of a sample size to understand all factors that affect a dynamo. In particular, mantle dynamics are confounding. Earth and Venus have the same size but Earth has plate tectonics, which cools the deep interior relatively quickly and thus helps drive a dynamo. Surface water is expected to help initialize plate tectonics (e.g., Korenaga, 2012), so a magnetic field may indirectly signal the habitability of the surface. That is, one could speculate that detecting a magnetosphere would reveal that a super-Earth is a true Earth-analogue.

Some previous studies suggested that super-Earths are unlikely to host a dynamo regardless of surface conditions and the mode of mantle dynamics. For example, Gaidos et al. (2010) asserted that cores in planets more massive than ~2–3 Earth-masses do not crystallize from the middle outwards, meaning that an inner core would never nucleate. Earth's inner core is a dominant source of power for our dynamo today (e.g., Labrosse, 2015; Nimmo, 2015)—the absence of an inner core in super-Earths would reduce the longevity of any dynamo. Relatedly, Tachinami et al. (2011) assumed that the mantles of super-Earths above ~2–3 Earth-masses are incredibly viscous, which leads to elevated temperatures in the lower mantle and thus a tiny thermal contrast across the core-mantle boundary (CMB). Shallow thermal gradients at the CMB translate into low heat flow, which implies that the metallic core would cool via thermal conduction without the vigorous fluid motions that are required to produce a dynamo. However, the mineral physics assumed in these studies contrasts with some recent work.

Recent work predicts that super-Earths are in fact likely to support dynamos, especially if they are true Earth-analogues. An inner core is not always necessary to generate a magnetic field. Indeed, Earth's inner core likely did not exist for most of our dynamo's lifetime (e.g., Bono et al., 2019; Labrosse, 2015). Driscoll & Olson (2011) determined that thermal convection alone can produce magnetic fields on the surfaces of super-Earths that are twice as strong as Earth's surface field—if their mantle dynamics efficiently cool the metallic core. Indeed, the viscosity of silicates in the lower mantles of super-Earths is highly uncertain but might not be much higher than in Earth's lower mantle (e.g., Karato, 2011; Stamenković et al., 2012). Van Summeren et al. (2013) found that massive Earth-analogues (i.e., with plate tectonics) could have strong dynamos that persist for billions of years powered by either thermal or compositional convection. In contrast, massive Venus-analogues (i.e., without plate tectonics) would only have (weak) dynamos once an inner core crystallized and kickstarted compositional convection. Crucially, Boujibar et al. (2020) found that state-of-the-art equations of state for iron alloys imply that metallic cores of super-Earths should crystallize from the center outwards—forming an inner core. The temperature range over which a super-Earth hosts an inner core expands as planetary mass increases, meaning that massive exoplanets could be likely to have inner cores.

The purpose of this study is to quantify the energetics of core-hosted dynamos in super-Earths. Recent studies provide detailed models for the internal structure of super-Earths (e.g., Boujibar et al., 2020; Noack & Lasbleis, 2020; Unterborn & Panero, 2019). Here we use thermodynamics to calculate if a dynamo may exist given the overall cooling rate of the metallic core. We aim to answer three questions: Are massive super-Earths relatively more or less likely to host dynamos? Does the presence of an inner core substantially increase the likelihood of a dynamo? How might observations of a dynamo discriminate between Earth- and Venus-analogues?

2 Theory and Numerical Methods

Our three-step approach provides the energetic requirements for dynamos in the metallic cores of super-Earths. First, we derive the radial profiles of density and pressure in the core. We consider planets with masses from 1 to 10 Earth-masses (M_E) in increments of 1 M_E. As in Earth, the mass of the core equals 32.5% of the planetary mass. We integrate the fundamental equations of planetary structure to obtain self-consistent descriptions of the internal structure. Second, we fit those radial profiles to polynomial equations that are amenable to analytic manipulations. These equations are used to parameterize the different sources and sinks of energy in the core. Finally, we calculate the critical heat flow required to drive a dynamo (Q_{min}) as a function of the radius of the inner core. If thermal buoyancy alone powered convection, then Q_{min} would equal the adiabatic heat flow (Q_{ad}). The adiabatic heat flow is what thermal conduction would transport up the thermal gradient in the core that convection nearly maintains—often called the “adiabat” because it represents how fluid parcels cool as they rise without exchanging heat (or entropy) with their surroundings. However, growth of the inner core and other sources of chemical buoyancy can lower Q_{min} substantially below Q_{ad}, typically by a factor of ~2.

The following sub-sections describe our approach in detail. Key references that provide the foundation for this study include Boujibar et al. (2020), Labrosse (2015), and O’Rourke (2020). Figure 1 shows the critical parameters that define the structure and evolution of the core. Table 1 lists the constants derived for cores with different masses. Table 2 defines the variables that are tracked to describe the energetics and thermochemical evolution of the core.

2.1 Structure of planetary cores

Our first task is to discover how density and pressure vary with depth within the metallic cores of super-Earths with different planetary masses. For any planetary body, the general approach is to integrate three equations (e.g., Boujibar et al., 2020; Seager et al., 2007; Sotin et al., 2007; Unterborn & Panero, 2019; Valencia et al., 2006). First, we consider conservation of mass:

$$\frac{dm}{dr} = 4\pi r^2 \rho. \tag{1}$$

Here $m(r)$ is the mass enclosed inside a sphere with radius r and ρ is density. Pressure increases with depth according to hydrostatic equilibrium:

$$\frac{dP}{dr} = -\rho g. \tag{2}$$

Here P is pressure. Gravitational acceleration is calculated self-consistently as $g(r) = Gm(r)/r^2$, where G is the gravitational constant. Finally, we need an equation of state that relates pressure and density. We use a Vinet equation of state for liquid iron (Boujibar et al., 2020):

$$P = 3K_{0V}\eta^{\frac{2}{3}}\left(1-\eta^{-\frac{1}{3}}\right)\exp\left[\frac{3}{2}(K_{1V}-1)\left(1-\eta^{-\frac{1}{3}}\right)\right]. \tag{3}$$

Here K_{0V} = 125 GPa and K_{1V} = 5.5 are the bulk modulus and its pressure-derivative, respectively, and $\eta = \rho/\rho_{0V}$ is the ratio of density (ρ) to a zero-pressure density (ρ_{0V} = 7700 kg/m^3). These parameters are consistent with recent experiments on an iron-sulfur alloy with ~7 wt% Si (Wicks et al., 2018). For simplicity, we ignore the effects of temperature on the equation of state.

We use an iterative method to obtain a self-consistent model. First, we guess $P(0)$, the pressure at the center of the core. We numerically integrate Equations 1–3 starting at the center in radial increments of 1 km. As radius increases, P decreases and $m(r)$ increases. The outer boundary of the core is reached when $m(R_C) = 0.325M_P$, where R_C is the radius of the core and M_P is the mass of the planet. Unterborn & Panero (2019) found that the pressure at the CMB should equal

$$P(R_C) = 1\text{ GPa}\left[262\left(\frac{\mathrm{R_P}}{R_E}\right) - 550\left(\frac{R_P}{R_E}\right)^2 + 432\left(\frac{R_P}{R_E}\right)^3\right]. \tag{4}$$

Here R_P is the radius of the super-Earth and R_E is the radius of Earth. We assume that $R_P = R_E(M_P/M_E)^{0.27}$ (Valencia et al., 2006). We use the bisection method to change our guess for $P(0)$ until the value of $P(R_C)$ agrees with Equation 4 within 0.05%.

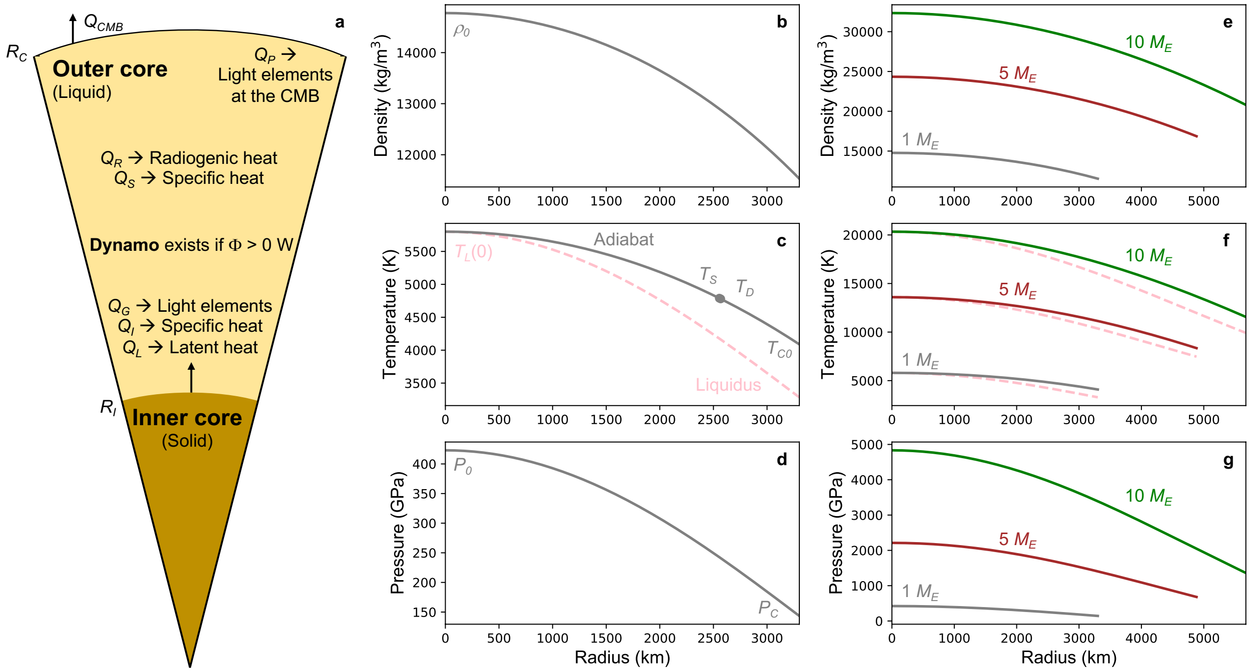

Figure 1. Internal structure of the core. Our goal is to obtain analytic equations for density, temperature, and pressure as a function of radius. To start, the core is entirely liquid and chemically homogenous. (a) As it cools, an inner core begins to cool from the center outwards. The total heat flow across the core-mantle boundary (Q_{CMB}) is partitioned between six different energy terms in the outer core (Q_P, Q_R, Q_S, Q_G, Q_I, and Q_L). Grey lines in the middle panels show the radial profiles of (b) density, (c) temperature, and (d) pressure in a 1 Earth-mass (M_E) planet. Here the temperature at the core-mantle boundary (T_{C0}) is chosen so the inner core is on the cusp of nucleating. The adiabat (grey line) intersects the liquidus (pink, dashed line) at the center of the core, i.e., at temperature $T_L(0)$. The right-hand panels show the radial profiles of (e) density, (f) temperature, and (g) pressure for 1 M_E (grey), 5 M_E (brown), and 10 M_E (green) planets. These internal structures are nearly identical to those in Boujibar et al. (2020) except we neglected thermal effects and did not model the mantle.

Once the basics of the internal structure are determined, we calculate other key thermodynamic properties. The Grüneisen parameter and the coefficient of thermal expansion vary with depth as $\gamma(r) = 1.6\eta^{0.92}$ and $\alpha(r) = (4 \times 10^{-6}\ \mathrm{K}^{-1})\eta^{-3}$, respectively (Boujibar et al., 2020). We take the volume-averaged values of $\gamma(r)$ and $\alpha(r)$ as representative of the entire core. Next, the liquidus (melting) temperature at the center of the core is $T_L(0) = (5800\ \mathrm{K})[P(0)/(423\ \mathrm{GPa})]^{0.515}$ and its pressure-derivative is $\mathrm{d}T_L/\mathrm{d}P = (9\ \mathrm{K\ GPa}^{-1})[P(0)/(423\ \mathrm{GPa})]^{-0.485}$ (Boujibar et al., 2020; Stixrude, 2014). Again, this liquidus is appropriate for cores containing several wt% of impurities such as silicon and other light elements in the iron alloy.

Table 1
Definitions of Key Model Outputs

Variable	Definition	Units
Structure and composition of the core		
t	Time	Gyr
k_C	Thermal conductivity of the core	W/m/K
P_P	Precipitation rate of light elements at the core-mantle boundary	1/K
[K]	Abundance of potassium in the core	ppm
R_I	Radius of the inner core	km
$T_L(R_I)$	Liquidus temperature at the inner core boundary	K
T_D	Average temperature in the outer core	K
T_S	Temperature associated with specific heat in the outer core	K
T_C	Temperature at the core-mantle boundary	K
Heat budget for the outer core		
Q_{CMB}	Total heat flow across the core-mantle boundary	TW
Q_S	Specific heat in the core	TW
Q_R	Radiogenic heat in the core	TW
Q_P	Gravitational heat from precipitation of light elements at the core-mantle boundary	TW
Q_G	Gravitational heat from exclusion of light elements from the inner core	TW
Q_L	Latent heat from the growth of the inner core	TW
Q_I	Heat flow across the inner core boundary	TW
Dissipation budget for the outer core (n.b., a dynamo exists if $\Phi > 0$ TW)		
Φ	Total dissipation available for a dynamo	TW
Φ_S	Dissipation associated with specific heat	TW
Φ_R	Dissipation associated with radiogenic heat	TW
Φ_P	Dissipation associated with the precipitation of light elements	TW
Φ_G	Dissipation associated with light elements from the inner core	TW
Φ_L	Dissipation associated with latent heat of the inner core	TW
Φ_I	Dissipation associated with cooling of the inner core	TW
Φ_K	Dissipation sink associated with thermal conduction in the outer core	TW
Q_{ad}	Minimum value of Q_{CMB} required to drive a dynamo in the outer core with thermal convection	TW
Q_{min}	Minimum value of Q_{CMB} required to drive a dynamo in the outer core with chemical convection	TW

Finally, we formulate parameterizations of density and temperature that are convenient to use in the rest of our model. The radial profile for density is fit to a fourth-order polynomial:

$$\rho(r) = \rho_0 \left[1 - \left(\frac{r}{L_\rho}\right)^2 - A_\rho \left(\frac{r}{L_\rho}\right)^4\right], \tag{5}$$

where L_ρ is a length scale and A_ρ is a fitting constant (Labrosse, 2015). To quantify how density changes with pressure, we can define an effective bulk modulus as $K_0 = 2\pi G(L_\rho\rho_0)^2/3$ and the derivative of the bulk modulus as $K_1 = (10A_\rho + 13)/5$. Note that K_0 and K_1 are not the same as the K_{0V} and K_{1V} used in the Vinet equation of state (Eq. 3), although they have the same dimensions and comparable, but not equal, values. Temperature is assumed to follow an isentropic (adiabatic) profile in the outer core, so $T(r) = T(0)[\rho(\mathrm{r})/\rho_0]^\gamma$.

2.2 Energy budget for the core

A dynamo may exist if there is enough energy in the outer core to power vigorous convection. We assume that the planetary rotation rate is fast enough for the Coriolis force to organize convective flow in the core (e.g., Stevenson, 2003, 2010). Either thermal or chemical buoyancy can provoke convection. Thermal convection occurs when hot material rises while cold material sinks. Chemical reactions can add or remove light elements from the iron alloy, providing chemical buoyancy that can assist thermal buoyancy or compensate for its absence. Our approach to assessing the energy budget follows many previous studies (e.g., Labrosse, 2015; Nimmo, 2015a, 2015b). The most important parameter is the total heat flow across the core-mantle boundary (Q_{CMB}), which must exceed a critical value (Q_{min}) to drive convection and thus a dynamo. Ultimately, mantle dynamics control Q_{CMB}, which depends on how fast solid-state convection in the mantle transports heat upwards from its lower boundary. Detailed simulations of mantle dynamics are complex, uncertain, and beyond the scope of this study. Our goal is to determine how large Q_{CMB} must be to sustain a dynamo, so we test a wide range. In the core, Q_{CMB} represents individual contributions from six individual sources:

$$Q_{CMB} = Q_S + Q_R + Q_P + Q_G + Q_L + Q_I. \quad (6)$$

Exact formulas for all terms on the right side of this equation are found in Labrosse (2015). They are unwieldy polynomials derived by integrating combinations of the density and temperature profiles over the volume of the outer core. Rather than wallow in the gory details, we explain the meaning of each term and how they relate to thermodynamic properties of the core.

The first three terms are important regardless of whether an inner core exists. First, Q_S represents the specific heat of the core. This term is directly proportional to the mass of the outer core and its rate of secular cooling, meaning the rate at which the absolute temperature of the core decreases ($\mathrm{d}T_C/\mathrm{d}t$). Second, Q_R is radiogenic heating in the outer core. Potassium is probably the primary source of radiogenic heating in the core, although uranium and thorium may contribute a minor amount of additional heating (e.g., Blanchard et al., 2017; Chidester et al., 2017). We assume that potassium is incompatible in the inner core. The concentration of potassium in the outer core increases as the inner core grows. Third, Q_P is associated with chemical precipitation at the CMB. Certain elements such as silicon, oxygen, and magnesium become less soluble in iron alloys at colder temperatures (e.g., Badro et al., 2016, 2018; Du et al., 2019; Hirose et al., 2017). When they precipitate, they move into the lower mantle and leave behind dense fluid. This process releases gravitational energy that promotes chemical convection in the core (e.g., Buffett et al., 2000; O'Rourke & Stevenson, 2016). We assume that the mass flux of precipitated material equals a constant (P_P) multiplied by $\mathrm{d}T_C/\mathrm{d}t$ and the mass of the outer core. Heat conducted along the adiabatic *within* the outer core is not included in Equation 6.

The final three terms in Equation 6 are related to the inner core. Light elements such as silicon and oxygen are incompatible in solid iron. As the core freezes from the center outwards, they are excluded from the inner core and represent a flux of light material into the base of the outer core. While precipitation at the CMB drives chemical convection from above, Q_G is a gravitational energy term that represents chemical convection driven from below. Crystallization of the inner core also involves latent heat (Q_L). Finally, we assume that the inner core has infinite thermal conductivity. Its temperature then equals $T_L(R_I)$, the liquidus temperature at the inner core boundary. The last term in Eq. 6 (Q_I) is the heat flux associated with this cooling. The opposite, end-member assumption made in some studies is that the inner core is perfectly insulating and Q_I = 0 TW (Labrosse, 2015). Either assumption is fine considering that Q_I is small compared to the other terms in the heat budget.

2.3 Dissipation budget for a dynamo in the core

Using the energy budget for the outer core, we calculate the total dissipation available to power a dynamo. Our models assume that a dynamo exists if there is any positive dissipation. In reality, the total dissipation must exceed the amount of Ohmic heating caused by the electrical resistance of the core fluid (e.g., Christensen, 2010). Ohmic losses are poorly constrained but could be quite large (e.g., Stelzer & Jackson, 2013). Our calculations thus provide a lower bound on the energetic requirements for a dynamo. Crucially, an "instantaneous" value for Q_{CMB} is used to calculate Φ because the free decay time for a planetary dynamo is only ~10^4 years (e.g., Stevenson, 2003, 2010). Various scaling laws are available to convert Φ into a dipole moment and then an intensity for the magnetic field at the surface (e.g., Aubert et al., 2009; Landeau et al., 2017). This study is chiefly concerned with the existence (or not) of a dynamo. Roughly speaking, $\Phi \sim$ 1–10s TW may translate into surface fields of ~10–100s μT.

The dissipation budget, like the heat budget, is partitioned into different terms. Each term in the heat budget has a counterpart in the dissipation budget that is labeled with the same subscript. The dissipation budget is derived from the combination of the energy budget (Eq. 6) and the entropy budget (e.g., Eq. 29 in Labrosse, 2015). Thermal conduction inside the outer core does not appear in the energy budget. However, thermal conduction is a sink of entropy and thus appears in the dissipation budget. In total,

$$\Phi = \Phi_S + \Phi_R + \Phi_P + \Phi_G + \Phi_L + \Phi_I - \Phi_K. \tag{7}$$

We assume that a dynamo exists if $\Phi > 0$ W. Again, the complicated polynomials that define each term are found in Labrosse (2015). We do not repeat the laborious algebra here. The key point is that each dissipation term (Φ_i) equals the corresponding energy term (Q_i) multiplied by a dimensionless efficiency factor that depends on whether the energy term is predominantly thermal or chemical. Thermal terms (subscripts S, R, L, and I) have "Carnot-like" efficiencies:

$$\Phi_i = \frac{T_D(T_i - T_C)}{T_i T_C} Q_i, \tag{8}$$

where T_D is the average temperature in the core (Figure 1c), T_C is the temperature at the CMB, and T_i is an effective temperature associated with the dissipation of each energy source. Radiogenic heating is uniformly distributed within the outer core so $T_R = T_D$. The effective temperature associated with secular cooling (T_S) is slightly hotter, but typically only by a few degrees. Both T_L and T_I equal $T_L(R_I)$, the temperature at the inner core boundary. Compared to thermal buoyancy, chemical effects are very efficient at driving convection. Quantitatively, the efficiency factors for Φ_P and Φ_G equal T_D/T_C, which is larger by a factor of ~2–10 than those from Equation 8. The dissipation sink associated with conduction (Φ_K) is directly proportional to T_C and the thermal conductivity of the core (k_C). For completeness, the full dissipation budget is

$$\Phi = \frac{T_D(T_S - T_C)}{T_S T_C} Q_S + \frac{T_D - T_C}{T_C} Q_R + \frac{T_D}{T_C}(Q_P + Q_G) + \frac{T_D[T_L(R_I) - T_C]}{T_L(R_I) T_C}(Q_L + Q_I) - \Phi_K. \quad (9)$$

Ultimately, thermal terms dominate the heat budget (e.g., $Q_S >> Q_G$) but chemical terms can dominate the dissipation budget (e.g., $\Phi_G >> \Phi_S$).

The adiabatic heat flow (Q_{ad}) is the minimum required to power a dynamo via thermal convection in the absence of chemical buoyancy. If there is no radiogenic heating, Q_{ad} precisely equals the heat flow that thermal conduction would transport up the isentropic temperature gradient in the core (i.e., the gradient that vigorous convection nearly maintains). Non-zero radiogenic heating decreases Q_{ad}. We calculate Q_{ad} by reducing the global heat budget to $Q_{CMB} = Q_S + Q_C$ and then solving for Q_{CMB} in Eq. 8 with all terms except Φ_S, Φ_R and Φ_K equal to zero:

$$Q_{ad} = \frac{T_S T_C}{T_D(T_S - T_C)} \Phi_K + \left[1 - \frac{T_S(T_D - T_C)}{T_D(T_S - T_C)}\right] Q_R. \quad (10)$$

Again, Φ_K is directly proportional to thermal conductivity and increases with planetary mass. Consult Equations A.20 to A.23 in Labrosse (2015) for the exact definition. The coefficient in front of Q_R equals ~10^{-2} typically, meaning that radiogenic heat does not help drive a dynamo unless that heat is removed from the core. Large amounts of radiogenic heating may increase Q_{CMB} by keeping the core at a higher temperature than the lower mantle. However, Eq. 10 is defined by assuming that Q_{CMB} is fixed. It is not obvious from Eq. 10 if Q_{ad} should increase or decrease as the inner core grows. On one hand, Φ_K is integrated over the volume of the outer core and thus must decrease as the core freezes. On the other hand, all the temperatures (T_S, T_C, and T_D) decrease as the core cools. Thermal conductivity is not temperature-dependent in our model. In reality, there should be a second-order compositional effect associated with inner core growth: the thermal conductivity of the core could decrease as the inner core grows because adding light elements to liquid iron alloys decreases the thermal conductivity relative to that for pure iron (e.g., Pozzo et al., 2012; Seagle et al., 2013; Zhang et al., 2021).

Table 2
Structural parameters for the metallic cores of super-Earths were computed using well-established methods.

			Planetary Mass (M_P) in Units of Earth-Masses (M_E)									
Term	**Units**	**Description**	**1**	**2**	**3**	**4**	**5**	**6**	**7**	**8**	**9**	**10**
M_C	10^{24} kg	Total mass of the core	1.94	3.88	5.82	7.76	9.70	11.6	13.6	15.5	17.5	19.4
R_P	km	Radius of the planet	6371	7682	8571	9263	9839	10335	10774	11170	11531	11863
R_C	km	Radius of the core	3301	3940	4343	4643	4884	5086	5261	5413	5551	5675
ρ_0	kg/m^3	Density at the center of the core	14775	17837	20290	22419	24339	26117	27787	29364	30879	32341
K	GPa	Effective bulk modulus	1657	2881	4097	5310	6529	7757	8995	10234	11490	12758
K'		Derivative of the effective bulk modulus	3.548	3.162	2.948	2.806	2.703	2.620	2.559	2.505	2.460	2.421
L_ρ	km	Length scale in the density profile	7372	8051	8438	8696	8881	9021	9130	9216	9285	9342
A_ρ		Constant in the density profile	0.474	0.281	0.174	0.103	0.0516	0.0116	-0.0206	-0.0474	-0.0701	-0.0897
$P(0)$	GPa	Pressure at the center of the core	423	834	1273	1733	2212	2707	3219	3742	4282	4834
P_C	GPa	Pressure at the core/mantle boundary	144	273	408	546	683	822	959	1097	1234	1370
γ		Grüneisen parameter (mass-weighted average)	1.41	1.38	1.36	1.34	1.33	1.32	1.31	1.30	1.29	1.28
$T_L(0)$	K	Liquidus temperature at the center of the core	5800	8227	10229	11991	13596	15087	16494	17824	19106	20337
$T_C(0)$	K	CMB temperature when the inner core nucleates	4089	5474	6579	7528	8346	9085	9765	10399	10994	11560
$\mathrm{d}T_L/\mathrm{d}P$	K/GPa	Change in liquidus temperature with pressure	9	7	5	5	4	4	4	3	3	3
g_C	m/s^2	Gravitational acceleration at the core/mantle boundary	11.9	16.7	20.6	24.0	27.1	29.9	32.7	35.3	37.9	40.2
α_T	10^{-5}/K	Coefficient of thermal expansion (mass-weighted average)	2.7	2.5	2.4	2.3	2.2	2.2	2.1	2.1	2.0	2.0

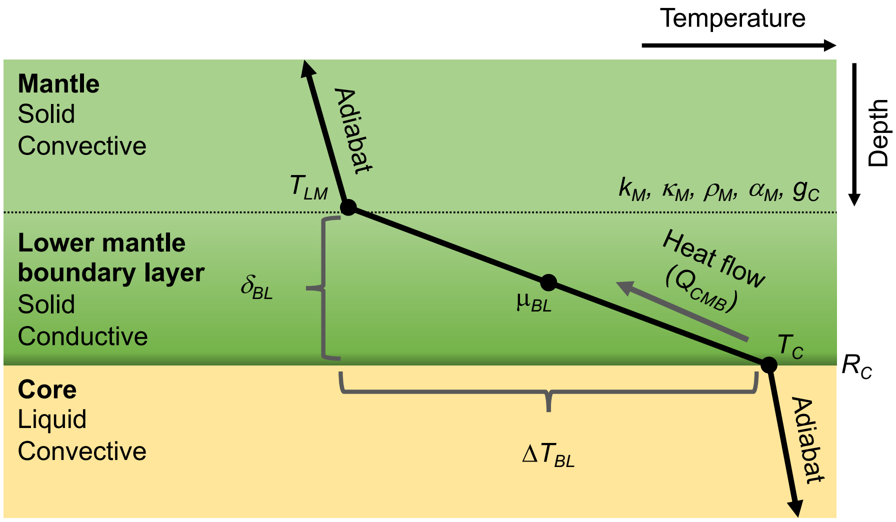

Figure 2. Cartoon of the boundary layer at the base of the solid mantle. We use a standard model based on the properties of this boundary layer to estimate how the heat flow across the core-mantle boundary (Q_{CMB}) scales with planetary mass. The other variables noted in this cartoon are defined in the main text. Note that a thermal boundary layer exists also at the top of the core. However, the core-side boundary layer is several orders of magnitude thinner than the boundary layer in the lower mantle—insignificant on the scale of this cartoon—because the solid mantle is >20 orders of magnitude more viscous than the liquid core.

2.4 Parameterizing the actual cooling rate of the metallic core

Our energetic calculations treat the heat flow across the CMB as a free parameter. However, we want to compare the minimum heat flow required to sustain a dynamo (Q_{min} and Q_{ad}) to some estimate of Q_{CMB}. In general, convection in the solid-state mantle regulates how fast heat is transported out of the deeper interior. Here we adapt a basic model that has been used for decades (e.g., Foley & Driscoll, 2016; Stevenson et al., 1983). We assume that a thermal boundary layer exists at the base of the solid, convecting mantle (Figure 2). The thermal contrast across that layer (ΔT_{BL}) is the difference between the temperature at the CMB (T_C) and the temperature in the lower mantle immediately above the boundary layer (T_{LM}). Heat flows out of the core and through this boundary layer according to Fourier's law:

$$Q_{CMB} = 4\pi R_C^2 k_M \left(\frac{\Delta T_{BL}}{\delta_{BL}}\right), \quad (11)$$

where k_M is the thermal conductivity of the lower mantle and δ_{BL} is the thickness of the boundary layer. In steady state, δ_{BL} is set by the criterion for convective instability, the Rayleigh number:

$$\mathrm{Ra} = \frac{\rho_M g_C \alpha_M \Delta T_{BL} \delta_{BL}^3}{\kappa_M \mu_{BL}}. \tag{12}$$

Here ρ_M, α_M, and κ_M are the density, coefficient of thermal expansion, and thermal diffusivity in the lower mantle, respectively. The average viscosity (μ_{BL}) is evaluated at the average temperature in the boundary layer. Fluid dynamical experiments and simulations show that the layer becomes unstable to convection when Ra ~ Ra_c ~ 10^3. If Ra > Ra_c, then the layer breaks away into a rising mantle plume. If Ra < Ra_c instead, then the layer continues to grow by thermal conduction. Therefore, the equilibrium thickness of the boundary layer is

$$\delta_{BL} = \left(\frac{\rho_M g_C \alpha_M \Delta T_{BL}}{\kappa_M \mu_{BL} \mathrm{Ra}_c}\right)^{\frac{1}{3}}. \tag{13}$$

Substituting Eq. 13 into Eq. 11 yields the classic formula for the total heat flow:

$$Q_{CMB} = 4\pi R_C^2 k_M \left(\frac{\rho_M g_C \alpha_M}{\kappa_M \mathrm{Ra}_c}\right)^{\frac{1}{3}} \mu_{BL}^{-\frac{1}{3}} \Delta T_{BL}^{\frac{4}{3}}. \tag{14}$$

To determine how Q_{CMB} scales with planetary mass, we analyze the individual terms that have significant mass-dependence (i.e., everything but 4π and Ra_c). Some of these terms (e.g., R_C and g) are calculated directly in this study, while the rest of the terms are estimated using the existing literature. Ultimately, we seek power-laws for Q_{CMB}, Q_{ad}, and Q_{min}:

$$\frac{Q(M_P)}{Q(M_E)} = \left(\frac{M_P}{M_E}\right)^{\Sigma}, \tag{15}$$

where Σ is a power-law exponent.

3 Results

3.1 Energetic requirements for a dynamo

Figure 3 shows how the inner core radius and the total heat flow across the core-mantle boundary affect the energetics of the core. More heat flow always provides more dissipation for the dynamo (Fig. 3a, 3b, and 3c). The required heat flow for a dynamo gradually increases with planetary mass. For planets of a certain mass, the minimum heat flow required for a dynamo is not extremely sensitive to the radius of the inner core. That is, Q_{ad} and Q_{min} have very similar values for R_I/R_C between ~0.1 and 0.7 for all planetary masses. However, there are some minor variations with inner core radius. Chemical convection can occur if $Q_{CMB} > Q_{min}$. For small inner cores ($R_I/R_C <$ ~0.1), Q_{min} rapidly decreases as R_I increases because the mass flux of light elements from the inner core grows like R_I squared. Because the mass of the inner core grows like R_I cubed, Q_{min} eventually flattens out and then starts to rise gradually. Thermal convection can occur if $Q_{CMB} > Q_{ad}$. Except when the inner core is very large, Q_{ad} increases with planetary mass. When R_I is >0.8R_C (1- and 5-M_E) or >0.65R_C (10-M_E), Q_{ad} starts to decrease because the total adiabatic heat flow decreases with the volume of the outer core.

The range of values for the total heat flow where chemical but not thermal convection may occur grows wider with increasing planetary mass. For a planet of one Earth-mass, the difference

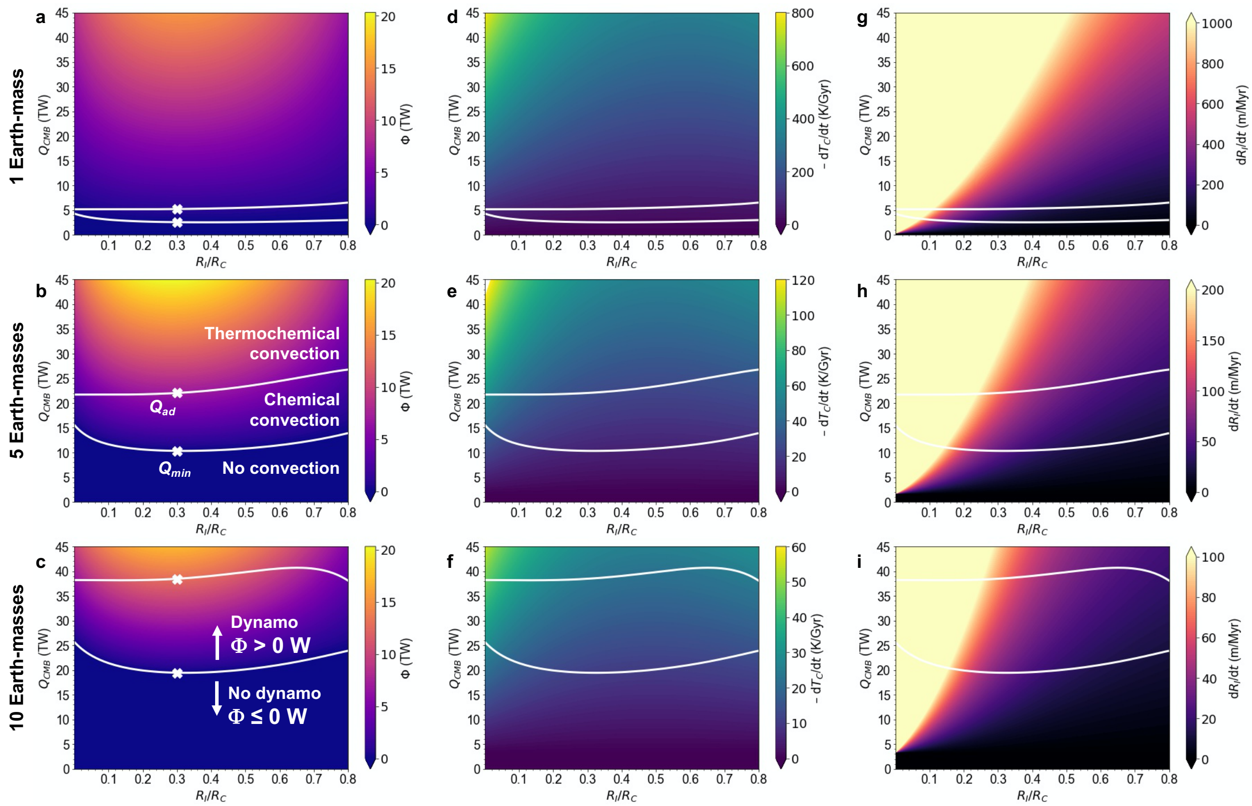

Figure 3. Self-consistent calculations for the energetics of the metallic cores of super-Earths. We vary two parameters: Q_{CMB}, the heat flow across the core-mantle boundary, and R_I/R_C, the normalized inner core radius. We calculated the total dissipation (color shading) available to drive a dynamo for 1 M_E (a), 5 M_E (b), 10 M_E (c) super-Earth exoplanets. Cross marks on Q_{min} and Q_{ad} in (a), (b), and (c) show how representative values are extracted for Table 3. White lines show the minimum heat flow required to produce chemical (Q_{min}, lower) and thermal (Q_{ad}, upper) convection. Subplots (d), (e) and (f) plot the rate at which the temperature of the core changes with time, while (g), (h), and (i) represent the growth rate of the inner core.

between Q_{ad} and Q_{min} is ~3 TW, while the difference in a planet of 10 Earth-masses is ~15–20 TW. The absolute value of the dissipation available for a dynamo (Φ) at a given Q_{CMB} stays approximately constant as planetary mass changes. While the dissipation for a dynamo increases slightly from 1 to 5 Earth-masses, it decreases from 5 to 10 Earth-masses (Fig. S1), resulting in very similar dissipation budgets across a spectrum of planetary masses. We did not directly calculate the magnetic field strengths associated with a certain dissipation because we are mostly concerned with the existence or non-existence of a dynamo. We might expect that magnetic fields for planets of various sizes would be similar in strength in the core. However, the surface fields of larger planets could be weaker as mantle thickness increases with planetary size.

As planetary mass increases, vastly more heat flow is required to change the temperature of the core or to increase the radius of the inner core. For example, Fig. 3d, 3e, and 3f shows that the value of dT_C/dt associated with a given Q_{CMB} decreases by a factor of ~7 as planetary mass increases from 1 to 5 Earth-masses and then decreases again by another factor of ~2 from 5 to 10 Earth-masses. Figure. 3g, 3h, and 3i illustrate how the growth rate of the inner core decreases drastically as planet mass increases. In Fig. 3g, the growth rate of the inner core is ~1 km/Myr

Table 3
We calculated the minimum heat flow required to sustain convection and thus a dynamo after the inner core nucleates (Q_{min}) and the adiabatic heat flow that would be required in the absence of radiogenic heating and/or chemical buoyancy (Q_{ad}). Different combinations of [K], P_P, and k_C were chosen to study the effects of these three parameters. We fit power laws to the results for each set of parameters to determine how the prospects for a dynamo scale with planetary mass.

	Nominal values. [K] = 50 ppm, $P_P = 5 \times 10^{-6}$ K^{-1}, k_C = 40 W/m/K		Radiogenic heating. [K] = 200 ppm, $P_P = 5 \times 10^{-6}$ K^{-1}, k_C = 40 W/m/K		Thermal conductivity. [K] = 50 ppm, $P_P = 5 \times 10^{-6}$ K^{-1}, k_C = 100 W/m/K		Precipitation at the CMB. [K] = 50 ppm, P_P = 0 K^{-1}, k_C = 40 W/m/K	
M_P (M_E)	Q_{ad} (TW)	Q_{min} (TW)	Q_{ad} (TW)	Q_{min} (TW)	Q_{ad} (TW)	Q_{min} (TW)	Q_{ad} (TW)	Q_{min} (TW)
1	5.2	2.6	5.3	3.1	13.1	6.2	5.2	2.7
2	9.7	4.8	9.7	5.9	24.1	11.4	9.7	5.0
3	13.8	6.4	13.9	8.2	34.5	15.1	13.8	6.7
4	17.6	8.7	17.7	10.9	43.8	20.5	17.6	9.2
5	22.0	10.3	22.3	13.3	55.0	24.3	22.0	10.8
6	24.9	12.3	25.3	15.8	62.1	29.1	24.9	13.2
7	28.3	14.5	28.8	18.5	70.5	34.3	28.3	15.8
8	32.1	15.2	32.8	20.1	79.9	35.6	32.1	16.0
9	35.3	17.4	36.2	22.7	88.0	40.7	35.3	18.5
10	38.5	19.5	39.4	25.3	95.7	45.7	38.5	21.0
Power law exponent	0.867 ± 0.006	0.872 ± 0.012	0.876 ± 0.005	0.906 ± 0.007	0.864 ± 0.006	0.863 ± 0.013	0.867 ± 0.006	0.887 ± 0.017

when the normalized core radius is 0.5 for Q_{CMB} ~ 40 TW. For those values of R_I/R_C and Q_{CMB}, the inner core growth rate is <200 and <50 m/Myr at 5 and 10 Earth-masses, respectively. This result means that massive cores will cool down very slowly over time. Relative to Earth and/or Venus, massive cores will take much longer to solidify, assuming that they start completely liquid (e.g., Boujibar et al., 2020). If their initial temperatures far exceed the liquidus, then an inner core might not nucleate for many billions of years. Sophisticated thermal evolution models are required to quantify these important timescales.

Table 3 lists representative values of Q_{ad} and Q_{min} for all planetary masses. We extracted these values at $R_I = 0.3R_C$ as noted in Fig. 3. We fit each column of values to power laws (Eq. 15) using the least-squares method and report the best-fit value and its standard deviation. The first column uses our nominal parameters: [K] = 50 ppm, $P_P = 5 \times 10^{-6}$ 1/K, and $k_C = 40$ W/m/K. The other three columns adjust each parameter individually to determine the sensitivity of our model. As we increase [K], Q_{ad} increases infinitesimally but Q_{min} increases significantly (Fig. S2). For a planet of 5 Earth-masses, Q_{ad} goes from 20.0 TW to 22.3 TW while Q_{min} increases from 10.3 TW to 13.3 TW. Thermal convection is less efficient than chemical convection, so increasing the proportion of radiogenic heating in the energy budget decreases the dissipation available for a dynamo at a constant total heat flow. Increasing k_C greatly increases both Q_{ad} and Q_{min} because Φ_K feeds into the definition of both values (Fig. S3). Planets of 5 Earth-masses see Q_{ad} increase from 22 TW to 55 TW and Q_{min} increase from 10.3 TW to 24.3 TW as k_C increases from 40 to 100 W/m/K. Changing the precipitation rate of light elements at the CMB does not change the Q_{ad} value by definition. Likewise, Q_{min} is not sensitive to the precipitation rate as long as an inner core exists with $R_I > \sim 0.05R_C$ (Fig. S4). That is, Q_G and Q_P are "substitute goods" in the dissipation budget. If Q_{CMB} is constant, then decreasing Q_P by adjusting P_P simply leads to a larger Q_G (e.g., a faster-growing inner core). Precipitation of light elements decreases the energetic for a dynamo by ~25% when there is no inner core. For example, for a 5 Earth-mass planet with $T_C = T_C(0) + 1$ K, Q_{CMB} must exceed 22 TW (Q_{ad}) for a dynamo in the absence of precipitation but only 15.7 TW with precipitation at our nominal rate.

Ultimately, the scaling laws for Q_{ad} and Q_{min} have the same power-law exponent (~0.9) regardless of uncertain values for properties such as thermal conductivity. This result means that we can potentially assess whether a super-Earth or a super-Venus is relatively more likely to host a dynamo than real Earth or Venus—even if we do not know the exact values of Q_{ad} and Q_{min} for these planets. The missing ingredient is a scaling law for the actual heat flow across the CMB.

3.2 Scaling laws for the heat flow across the core/mantle boundary

We constructed a scaling relation to describe how the cooling rate of the core changes with planetary mass. Equation 14 defines the heat flow across the CMB in terms of the properties of the boundary layer at the base of the solid mantle (Figure 2). We assume the eight mass-dependent terms in that equation obey a power laws of the form $X(M_P)/X(M_E) = (M_P/M_E)^x$, where x is a "power-law exponent," analogous to Equation 15. We combine all eight power-law exponents to calculate the final scaling relation:

$$Q_{CMB}(M_P) = Q_{CMB}(M_E)\left(\frac{M_P}{M_E}\right)^{2a+b+\frac{1}{3}(c+d+e)-\frac{1}{3}(f+g)+\frac{4}{3}(h)} . \qquad (16)$$

Table 4 shows that letters a, b, c, d, e, f, g, and h correspond to R_C, k_M, ρ_M, g_C, α_M, κ_M, μ_{BL}, and ΔT_{BL}, respectively. Table S1 lists our estimated values of these parameters at M_P = 1–10M_E. Power-law exponents for a and d, respectively associated with variables R_C and g, were derived from the values in Table 2. We report the best-fit value for each x and the formal uncertainty ("1-sigma") of the fit. Of course, the formal uncertainty is much smaller than the true uncertainty because the statistical fits are built on a series of assumptions.

Table 4
Exponents in the power laws that describe how various parameters may scale with planetary mass.

Variable	Definition	Power-Law Exponent
R_C	Radius of the core	$a = 0.234 \pm 0.003$
k_M	Thermal conductivity of the lower mantle	$b = 0.47 \pm 0.04$
ρ_M	Density of the lower mantle	$c = 0.23 \pm 0.01$
g	Gravitational acceleration near the core-mantle boundary	$d = 0.53 \pm 0.01$
α_M	Thermal expansivity of the lower mantle	$e = -0.69 \pm 0.03$
κ_M	Thermal diffusivity of the lower mantle	$f = 0.25 \pm 0.04$
μ_{BL}	Average viscosity in the lower mantle boundary layer	$g = -0.32 \pm 0.04$
ΔT_{BL}	Thermal contrast across the lower mantle boundary layer	$h = 0.57 \pm 0.02$
Q_{CMB}	Heat flow across the core-mantle boundary	1.7 ± 0.4

Here is how we derived the rest of the scaling relationships:

- <u>Thermal conductivity of the lower mantle (k_M).</u> The thermal conductivity of silicates, which includes contributions from radiative, electronic, and phonon terms, tends to increase with temperature. Figure 9b from Stamenković et al. (2011) shows thermal conductivity as a function of pressure up to >1 TPa, assuming an adiabatic increase in temperature with pressure. We extracted values at the pressure of the CMB (P_C) for each planet from that plot.

- Density of the lower mantle (ρ_M). We calculated the density of (Mg,Fe)SiO_3 silicate at P_C using the polytropic equation of state from Seager et al. (2007) in their Table 3. Thermal effects that are not included in that equation may change silicate densities by a few percent, which is much smaller than the variations between differently sized planets.
- Thermal expansivity of the lower mantle (α_M). Following Boujibar et al. 2020, we assumed that $\alpha_M \propto (\rho_M)^{-3}$ and thus $e = -3c$. This scaling relationship does not depend on the actual value of α_M in Earth's mantle.
- Thermal diffusivity of the lower mantle (κ_M). We assume that the lower mantles of super-Earths are hot enough that their specific heats are near the Dulong-Petit limit and thus independent of planetary mass. In this case, $\kappa_M \propto k_M/\rho_M$ by definition and $f = b - c$.
- Thermal contrast across the lower mantle boundary layer (ΔT_{BL}). By definition, $\Delta T_{BL} = T_C - T_{LM}$. We calculate T_{LM} using Equation 7 in Unterborn & Panero (2019), which is the adiabatic temperature in the lower mantle assuming a potential temperature of 1600 K for the mantle. We set T_C equal to $T_C(0)$, meaning that our scaling law applies best to planets that are on the cusp of nucleating an inner core.
- Average viscosity in the lower mantle boundary layer (μ_{BL}). Following Section 5 in Valencia & O'Connell (2009), we assume that viscosity at a given pressure decreases with temperature according to an Arrhenius law. Specifically, we assume $\mu_{BL} \propto \exp[-20(1 - T_{BL}/T_{melt})]$, where $T_{BL} = T_C - 0.5\Delta T_{BL}$ and T_{melt} is the melting temperature of $MgSiO_3$ silicates at the pressure of the CMB (Stixrude, 2014). All relevant temperatures increase rapidly with planetary mass. However, the ratio T_{BL}/T_{melt} decreases from ~0.67 to 0.60 as mass increases from ~1–10M_E. The key point is that our formulation of viscosity implies that the temperature-dependence of viscosity is slightly more important than its pressure-dependence. Even at extreme pressures, viscosities could be similar to or less than those in the lower mantle of Earth (Karato, 2011). On the other hand, significant pressure-dependence could increase the viscosity by several orders of magnitude (e.g., Noack & Lasbleis, 2020; Stamenković et al., 2012), so the true uncertainty on this parameter is much larger than the formal error reported in Table 4.

Overall, we estimate that $Q_{CMB}(M_P)/Q_{CMB}(M_E) = (M_P/M_E)^{1.7\pm0.4}$ or, equivalently, that $\Sigma = 1.7 \pm 0.4$, which implies that the actual heat flow across the CMB increases rapidly in comparison to the minimum value required to sustain a dynamo in the metallic core.

Figure 4 compares the three scaling laws derived in this study for Earth- and Venus-analogue planets. In our Solar System, the solid mantle of Earth cools fast compared to that of Venus because plate tectonics efficiently transports internal heat to the surface. Most models predict that the mantle of Venus is thus hotter than Earth's at present day (e.g., Driscoll & Bercovici, 2013; Driscoll & Bercovici, 2014; O'Rourke et al., 2018). According to Eq. 14, increasing T_{LM} causes ΔT_{BL} and Q_{CMB} to decrease. Although the cores of Earth and Venus cool at different rates, we can use Eq. 16 to describe how the cooling rates of massive Earth- and Venus-analogues scale with planetary mass. For Earth, Q_{CMB} ~ 5–15 TW based on studies of mantle plumes and the thermal state of the basal mantle (e.g., Lay et al., 2008). Earth-analogue 1 (Figure 4a) has $Q_{ad} > Q_{CMB}$ ~ 10 TW > Q_{min} and thus a dynamo driven by chemical buoyancy. Earth-analogue 2 (Figure 4b) has Q_{CMB} ~ 6 TW > $Q_{ad} > Q_{min}$ and thus a dynamo sustained by both thermal and chemical buoyancy. In contrast, the internal heat budget of Venus is essentially unconstrained (e.g., Smrekar et al., 2018). Venus-analogues 1 (Figure 4c) and 2 (Figure 4d) are both tuned to have $Q_{CMB} < Q_{min}$ with Q_{CMB} ~ 6 and 2 TW, respectively. Figure 4a and 4c (analogues #1) assume that the thermal conductivity of the core is at the upper end of recent estimates (k_C ~ 100 W/m/K), while Figure 4b and 4d (analogues #2) assume that conventionally low values (k_C ~ 40 W/m/K) are correct. Ultimately, our inferences about the prospects for dynamos are not sensitive to the choice of thermal conductivity.

Earth-analogues grow increasingly likely to host a dynamo in their metallic cores as planetary mass increases. Earth-analogue 1 transitions from chemical to thermochemical convection where $M_P > 1.4\ M_E$ given the nominal power-law exponent of $\Sigma = 1.7$ in the scaling law for Q_{CMB} (Eq. 15). If the most optimistic scaling is adopted ($\Sigma = 2.1$), then the transition to $Q_{CMB} > Q_{ad}$ occurs when $M_P > 1.2\ M_E$. If Q_{CMB} increases relatively slowly with planetary mass ($\Sigma = 1.3$), then massive versions of Earth-analogue 1 still only need to rely on chemical buoyancy until $M_P > 1.9\ M_E$ to sustain a dynamo. Broadly speaking, Q_{min} increases with a power-law exponent of ~0.9 only, so massive planets are never *less* likely to host a dynamo than an Earth-mass analogue. Likewise, massive versions of Earth-analogue 2 should always host a dynamo in their metallic cores driven by, at least, thermal convection. Table 3 shows that the power-law exponents for Q_{min} and Q_{ad} remain ≤0.9 for different amounts of radiogenic heating ([K]) and with or without precipitation of light elements (P_P), meaning that our general statements about Earth-analogues are not sensitive to these under-constrained parameters.

Venus-analogues are also likely to host dynamos in their metallic cores above a certain planetary mass. Using the nominal power-law exponent for Q_{CMB} ($\Sigma = 1.7$), chemical convection in the core is expected to occur if $M_P > 1.0$ or $1.4\ M_E$ for Venus-analogues 1 and 2, respectively.

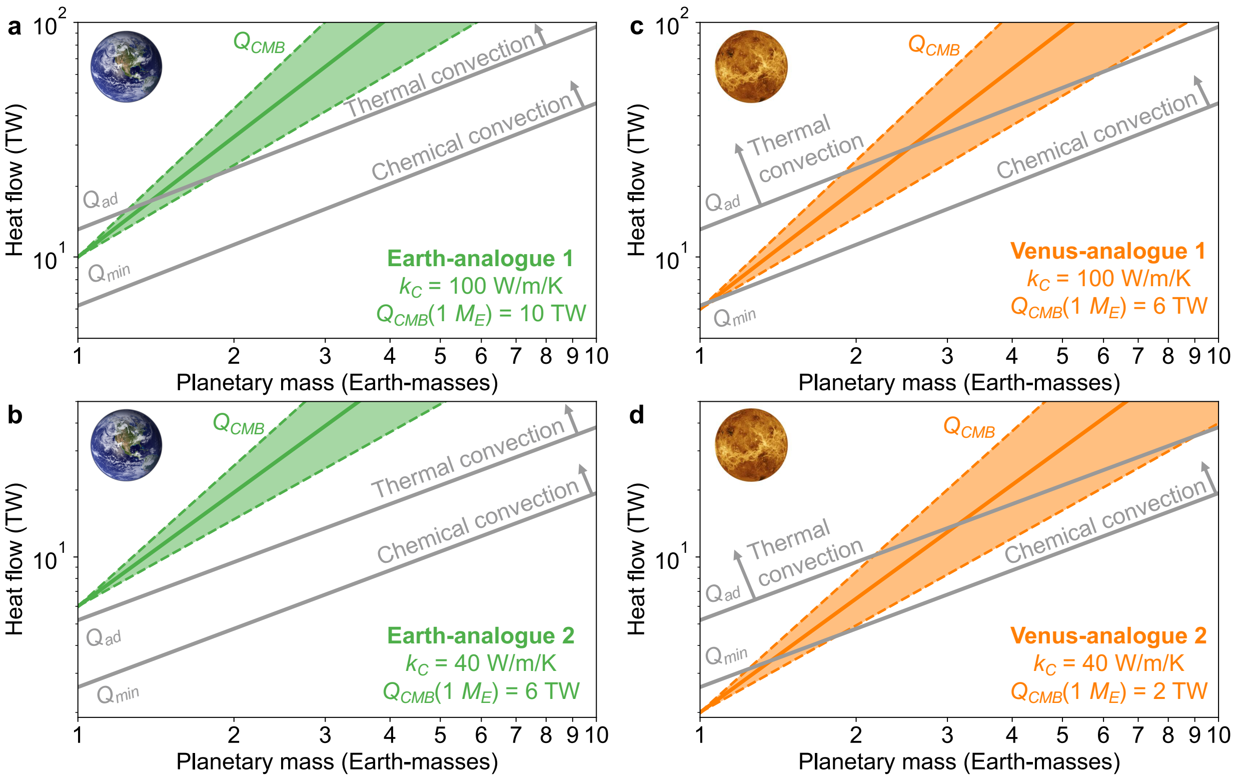

Figure 4. The likelihood of a dynamo in the metallic cores of rocky exoplanets may increase with planetary mass if their lower mantles are completely solid. Each subplot shows how the actual heat flow across the core-mantle boundary (Q_{CMB}) and the minimum values required to drive chemical (Q_{min}) and thermal convection (Q_{ad}) in the core scale with planetary mass. Solid lines show the nominal scaling for Q_{CMB}, and the shaded region bordered by dashed lines indicates the formal uncertainty from Table 3. The power-law fits for Q_{ad} and Q_{min} have negligible formal uncertainties. Crucially, the scaling law used for Q_{CMB} assumes that the lower mantle is solid. Panels (a) and (c) show how Earth- and Venus-analogues behave if the thermal conductivity of the core is relatively high ($k_C \sim 100$ W/m/K). Chemical convection powers Earth's dynamo if $Q_{CMB} \sim 10$ TW (a) while the core of Venus is cooling too slowly to convect (c). In contrast, panels (b) and (d) were generated using a lower thermal conductivity for the core ($k_C \sim 40$ W/m/K). Thermal convection can occur in Earth's core even if $Q_{CMB} \sim 6$ TW (b) while Venus still fails to host a dynamo if $Q_{CMB} \sim 2$ TW (d).

Thermal convection is also possible in the cores of very massive Venus-analogues (M_P > 2.5 to 3.1 M_E, respectively). If the power-law exponent for Q_{CMB} is Σ = 2.1, then ~1.9 M_E is the planetary mass at which both Venus-analogues could sustain dynamos powered by thermal convection. Even if the cooling rate of the core increases fairly slowly with planetary mass (Σ = 1.3), growth of the inner core could drive a dynamo if M_P > 1.1 or 1.8 M_E for Venus-analogues 1 and 2, respectively. Thermal convection would occur in this case for only the most massive Venus-analogues (M_P > 6.0 or 9.1 M_E). In other words, very massive exoplanets with solid mantles and no dynamo are likely Venus-analogues with no inner core.

Overall, our nominal scalings predict that both Earth- and Venus-analogues are predicted to have strong global magnetic fields for planetary masses exceeding ~1.4 Earth-masses. Growth of an inner core is essential to driving a dynamo in massive Venus-analogues, while massive Earth-analogues have enough energy for thermal convection. At smaller terrestrial planets, the presence of a magnetosphere may signal the operation of plate tectonics (i.e., at real Earth but not real Venus). However, magnetic fields—if they are ubiquitous for planets above a certain mass—may not always provide a unique probe into mantle dynamics.

4 Discussion

Any study of dynamos in exoplanets must rely on simplified assumptions and judicious speculation. Our models for the energy budgets of metallic cores are one step on a long path towards predicting the occurrence of planetary magnetism at exoplanets and, eventually, interpreting any detections. We concluded that massive planets are relatively likely to host dynamos in their metallic cores if their silicate mantles are entirely solid. Future studies could provide some straightforward augmentations of our modeling approach. For example, we only modeled planets with Earth-like core mass fractions (0.325) and Earth-like abundances of light elements (~6 wt%). Developing scaling laws for planets with Mercury-like (~0.68) and Mars-like (~0.20) core mass fractions and different amounts of impurities in the core would be an easy next step (e.g., Boujibar et al., 2020). Perhaps most importantly, the assumption that solid-state mantle convection directly governs the heat flow out of the core could be wildly inaccurate, which has big-picture implications for modeling massive Earth- and Venus-analogues.

4.1 Towards self-consistent models of thermal evolution

Our scaling law for the heat flow across the core-mantle boundary did not fully consider how the core and mantle cool together over time. Mantle convection tends to "self-regulate" so silicates at the surface are near their melting temperature, where mantle viscosity is minimal. As a result, super-Earths could have mantle potential temperatures that are similar within a few hundred degrees (e.g., O'Rourke & Korenaga, 2012; Stamenković et al., 2011, 2012; Tackley et al., 2013; Valencia & O'Connell, 2009). Of course, small differences in mantle temperatures can have dramatic effects on surface habitability. A few hundred K is the difference between catastrophic volcanism and a total dearth of volcanic and tectonic activity. However, the cores of massive super-Earths could be several thousand degrees hotter than the core of Earth because much more gravitational energy is released as heat during their formation (e.g., Boujibar et al., 2020; Noack & Lasbleis, 2020; Stixrude, 2014). The fact that T_C increases more rapidly than T_L with planetary mass is why we predict that super-Earths are relatively likely to host dynamos. However, T_C might decrease more rapidly with time relative to its initial value in super-Earths for the same reason (i.e., mantle viscosity is highly temperature-dependent). Mantle convection might also "self-regulate" to a particular thermal contrast above the core-mantle boundary. Future studies can address this issue with self-consistent models of the mantle and core.

4.2 Likelihood of a basal magma ocean

Our scaling law for the heat flow across the core-mantle boundary was built on the assumption that the silicate mantle is fully solidified. Indeed, Table S1 shows that the existence of an inner core implies temperatures at the top of the core that are below the melting point of silicates at the relevant pressures, according to one parameterization in Stixrude (2014). However, the melting temperature of silicates is highly sensitive to their composition. Boujibar et al. (2020) showed that an inner core may co-exist with a partially liquid lower mantle. If temperatures in the lower mantle are high enough, there could be a global layer of molten silicates called a basal magma ocean (BMO). Labrosse et al. (2007) proposed that Earth itself had a BMO that took a few billion years to solidify. O'Rourke (2020) speculated that a BMO may still exist within Venus today. A BMO would dramatically affect the heat and dissipation budgets for the metallic core.

Crucially, a BMO vastly reduces the cooling rate of the core because its specific and latent heat subtracts from the heat budget. In other words, the heat that we predicted the solid mantle would extract from the core would actually be the total amount of heat extracted from the BMO and the core. Because the BMO is a heat sink, the cooling rate of the core is decreased (e.g., by a factor of two or more). Models generally predict that a thick BMO reduces the heat flow out of the core to levels that are sub-critical for a dynamo (e.g., Blanc et al., 2020; Labrosse et al., 2007; O'Rourke, 2020; Ziegler & Stegman, 2013). However, the BMO itself may host a dynamo because liquid silicates are electrically conductive under extreme pressures and temperatures (e.g., Holmström et al., 2018; Scipioni et al., 2017; Soubiran & Militzer, 2018; Stixrude et al., 2020). Planets could transition from a BMO-hosted to a core-hosted dynamo over time as they cool (Ziegler & Stegman, 2013). Speculatively, a BMO-hosted dynamo could produce a stronger magnetosphere because the dynamo-generating region is closer to the surface. No study has yet modeled the prospects for a dynamo in the BMO of massive exoplanets—but such studies are obviously a very high priority. Our models for the energetics of metallic cores would easily interface with more detailed descriptions of the silicate mantle with or without a BMO.

5 Conclusions

Here we presented a model for the energetics of dynamos in the metallic cores of super-Earth exoplanets. The model is built on a one-dimensional (radial) parameterization of the density and pressure within the liquid portion of the core, which is assumed to maintain an adiabatic thermal gradient due to vigorous convection. The total dissipation available for a dynamo is calculated using the energy and entropy budgets for the core. Overall, we considered four sources of thermal buoyancy and two sources of chemical buoyancy that can help drive convection. We developed a simple scaling law to roughly estimate how the actual heat flow across the core-mantle boundary (CMB) may vary with planetary mass for comparison to the calculated values of the minimum heat flow required to sustain a dynamo with and without an inner core.

Our main conclusions are as follows:

1. The minimum heat flows necessary to provoke thermal and chemical convection both increase with planetary mass according to power laws with exponents of ~0.9. These scaling laws are insensitive to properties of the core such as its thermal conductivity, the rate at which light elements precipitate at the CMB, and the amount of radiogenic heating—all of which are uncertain even for Earth and impossible to directly constrain using available techniques for exoplanets.

2. An inner core vastly increases the likelihood of a dynamo, especially within massive planets. Fortunately, the critical heat flow required for a dynamo is not sensitive to the exact radius of the inner core. We lack direct constraints on the size of the inner core for any planetary body in our Solar System besides Earth, so measuring this parameter for exoplanets seems impossible in the foreseeable future.
3. The actual heat flow across the CMB is predicted to increase with planetary mass according to a power law with an exponent of ~1.7 for both Earth- and Venus-analogues. Of the eight terms that feed into this scaling law, viscosity is likely the most uncertain. We inferred that super-Earths have less viscous lower mantles than Earth, but other models predict that silicates become very viscous at extreme pressures. That said, viscosity would have to increase by the square of planetary mass (i.e., a 10 Earth-mass planet having 100 times the mantle viscosity of Earth) to reduce the power-law exponent to ~0.9 to match the scaling laws for the minimum heat flow to drive a dynamo.
4. As planetary mass increases, the predicted rates of temperature change and inner core growth both decrease rapidly. Because enormous cores are enormous heat sinks, inner cores may not nucleate for a long time unless core temperatures are initially near the liquidus.
5. Detecting a magnetic field would not prove that a super-Earth larger than ~1.4 Earth-masses is a true Earth-analogue. However, the absence of a magnetic field is still a good sign that a super-Earth does not have Earth-like mantle dynamics. Venus might have an inner core but no dynamo today. Scaled-up versions of Venus could sustain chemical convection in the core even in the absence of plate tectonics if they have an inner core. Thermal convection alone would probably not produce a dynamo in Venus-analogues smaller than ~3 Earth-masses. In contrast, virtually every massive Earth-analogue should host a dynamo even if an inner core has not yet nucleated.

Future studies should consider non-Earth-like compositions and core mass fractions—and should self-consistently model the thermal evolution of the core and mantle. Perhaps most importantly, a basal magma ocean in the lower mantle of a super-Earth would substantially decrease the heat flow out of the core relative to the scaling law we developed assuming a solid mantle. Because silicates within the basal magma ocean would be electrically conductive, the basal magma ocean itself could sustain a dynamo even as it suppresses convection within the core.

Acknowledgments

All the data sets required to create the Figures and Tables are available in the main text, the supporting information, and the repository platform *Open Science Framework* (*https://osf.io/xg8c2/?view_only=dd32f4a522124943a49b92cafcb8a563*). A Jupyter notebook that runs the models and produces Figure 3 and Table 3 is archived with the repository platform. *[Note for review: We will replace the view-only link with a permanent doi before the manuscript is accepted, after any major concerns are addressed.]*

References

Aubert, J., Labrosse, S., & Poitou, C. (2009). Modelling the palaeo-evolution of the geodynamo. *Geophysical Journal International*, *179*(3), 1414–1428. https://doi.org/10.1111/j.1365-246X.2009.04361.x

Badro, J., Siebert, J., & Nimmo, F. (2016). An early geodynamo driven by exsolution of mantle components from Earth's core. *Nature*, *536*(7616), 326–328. https://doi.org/10.1038/nature18594

Badro, J., Aubert, J., Hirose, K., Nomura, R., Blanchard, I., Borensztajn, S., & Siebert, J. (2018). Magnesium Partitioning Between Earth's Mantle and Core and its Potential to Drive an Early Exsolution Geodynamo. *Geophysical Research Letters*, *45*(24), 13,240-13,248. https://doi.org/10.1029/2018GL080405

Blanc, N. A., Stegman, D. R., & Ziegler, L. B. (2020). Thermal and magnetic evolution of a crystallizing basal magma ocean in Earth's mantle. *Earth and Planetary Science Letters*, *534*, 116085. https://doi.org/10.1016/j.epsl.2020.116085

Blanchard, I., Siebert, J., Borensztajn, S., & Badro, J. (2017). The solubility of heat-producing elements in Earth's core. *Geochemical Perspectives Letters*, 1–5. https://doi.org/10.7185/geochemlet.1737

Bono, R. K., Tarduno, J. A., Nimmo, F., & Cottrell, R. D. (2019). Young inner core inferred from Ediacaran ultra-low geomagnetic field intensity. *Nature Geoscience*, *12*(2), 143–147. https://doi.org/10.1038/s41561-018-0288-0

Boujibar, A., Driscoll, P., & Fei, Y. (2020). Super-Earth Internal Structures and Initial Thermal States. *Journal of Geophysical Research: Planets*, *125*(5), e2019JE006124. https://doi.org/10.1029/2019JE006124

Buffett, B. A., Garnero, E. J., & Jenaloz, R. (2000). Sediments at the Top of Earth's Core. *Science*, *290*(5495), 1338–1342. https://doi.org/10.1126/science.290.5495.1338

Chidester, B. A., Rahman, Z., Righter, K., & Campbell, A. J. (2017). Metal-silicate partitioning of U: Implications for the heat budget of the core and evidence for reduced U in the mantle. *Geochimica et Cosmochimica Acta*, *199*, 1–12. https://doi.org/10.1016/j.gca.2016.11.035

Christensen, U. R. (2010). Dynamo Scaling Laws and Applications to the Planets. *Space Science Reviews*, *152*(1–4), 565–590. https://doi.org/10.1007/s11214-009-9553-2

Dong, C., Jin, M., & Lingam, M. (2020). Atmospheric Escape From TOI-700 d: Venus versus Earth Analogs. *The Astrophysical Journal*, *896*(2), L24. https://doi.org/10.3847/2041-8213/ab982f

Driscoll, P., & Bercovici, D. (2013). Divergent evolution of Earth and Venus: Influence of degassing, tectonics, and magnetic fields. *Icarus*, *226*(2), 1447–1464. https://doi.org/10.1016/j.icarus.2013.07.025

Driscoll, P. E. (2018). Planetary Interiors, Magnetic Fields, and Habitability. In H. J. Deeg & J. A. Belmonte (Eds.), *Handbook of Exoplanets* (pp. 1–18). Springer International Publishing. https://doi.org/10.1007/978-3-319-30648-3_76-1

Driscoll, P, & Bercovici, D. (2014). On the thermal and magnetic histories of Earth and Venus: Influences of melting, radioactivity, and conductivity. *Physics of the Earth and Planetary Interiors*, *236*, 36–51. https://doi.org/10.1016/j.pepi.2014.08.004

Driscoll, Peter, & Olson, P. (2011). Optimal dynamos in the cores of terrestrial exoplanets: Magnetic field generation and detectability. *Icarus*, *213*(1), 12–23. https://doi.org/10.1016/j.icarus.2011.02.010

Du, Z., Boujibar, A., Driscoll, P., & Fei, Y. (2019). Experimental Constraints on an MgO Exsolution-Driven Geodynamo. *Geophysical Research Letters*, *46*(13), 7379–7385. https://doi.org/10.1029/2019GL083017

Foley, B. J., & Driscoll, P. E. (2016). Whole planet coupling between climate, mantle, and core: Implications for rocky planet evolution. *Geochemistry, Geophysics, Geosystems*, *17*(5), 1885–1914. https://doi.org/10.1002/2015GC006210

Foley, B. J., Bercovici, D., & Landuyt, W. (2012). The conditions for plate tectonics on super-Earths: Inferences from convection models with damage. *Earth and Planetary Science Letters*, *331–332*, 281–290. https://doi.org/10.1016/j.epsl.2012.03.028

Gaidos, E., Conrad, C. P., Manga, M., & Hernlund, J. (2010). Thermodynamic limits on magnetodynamos in rocky exoplanets. *Astrophysical Journal*, *718*(2), 596–609. https://doi.org/10.1088/0004-637X/718/2/596

Hirose, K., Morard, G., Sinmyo, R., Umemoto, K., Hernlund, J., Helffrich, G., & Labrosse, S. (2017). Crystallization of silicon dioxide and compositional evolution of the Earth’s core. *Nature*, *543*(7643), 99–102. https://doi.org/10.1038/nature21367

Holmström, E., Stixrude, L., Scipioni, R., & Foster, A. S. (2018). Electronic conductivity of solid and liquid (Mg, Fe)O computed from first principles. *Earth and Planetary Science Letters*, *490*, 11–19. https://doi.org/10.1016/j.epsl.2018.03.009

Kane, S. R., Kopparapu, R. K., & Domagal-Goldman, S. D. (2014). On the frequency of potential Venus analogs from Kepler data. *Astrophysical Journal Letters*, *794*(1). https://doi.org/10.1088/2041-8205/794/1/L5

Kane, S. R., Arney, G., Crisp, D., Domagal-Goldman, S., Glaze, L. S., Goldblatt, C., et al. (2019). Venus as a Laboratory for Exoplanetary Science. *Journal of Geophysical Research: Planets*, *124*(8), 2015–2028. https://doi.org/10.1029/2019JE005939

Karato, S. (2011). Rheological structure of the mantle of a super-Earth: Some insights from mineral physics. *Icarus*, *212*(1), 14–23. https://doi.org/10.1016/j.icarus.2010.12.005

Korenaga, J. (2012). Plate tectonics and planetary habitability: current status and future challenges. *Annals of the New York Academy of Sciences*, *1260*, 87–94. https://doi.org/10.1111/j.1749-6632.2011.06276.x

Labrosse, S. (2015). Thermal evolution of the core with a high thermal conductivity. *Physics of the Earth and Planetary Interiors*, *247*, 36–55. https://doi.org/10.1016/j.pepi.2015.02.002

Labrosse, S., Hernlund, J. W., & Coltice, N. (2007). A crystallizing dense magma ocean at the base of the Earth's mantle. *Nature*, *450*(7171), 866–9. https://doi.org/10.1038/nature06355

Landeau, M., Aubert, J., & Olson, P. (2017). The signature of inner-core nucleation on the geodynamo. *Earth and Planetary Science Letters*, *465*, 193–204. https://doi.org/10.1016/j.epsl.2017.02.004

Lay, T., Hernlund, J., & Buffett, B. A. (2008). Core–mantle boundary heat flow. *Nature Geoscience*, *1*(1), 25–32. https://doi.org/10.1038/ngeo.2007.44

Nimmo, F. (2015a). Energetics of the Core. In *Treatise on Geochemistry: Second Edition* (Vol. 1, pp. 31–65). Elsevier B.V. https://doi.org/10.1016/B978-044452748-6.00128-0

Nimmo, F. (2015b). Thermal and Compositional Evolution of the Core. In *Treatise on Geochemistry: Second Edition* (Vol. 9, pp. 217–241). Elsevier B.V. https://doi.org/10.1016/B978-044452748-6.00147-4

Noack, L., & Lasbleis, M. (2020). Parameterisations of interior properties of rocky planets: An investigation of planets with Earth-like compositions but variable iron content. *Astronomy and Astrophysics*, *638*. https://doi.org/10.1051/0004-6361/202037723

O'Rourke, J. G. (2020). Venus: A Thick Basal Magma Ocean May Exist Today. *Geophysical Research Letters*, *47*(4). https://doi.org/10.1029/2019GL086126

O'Rourke, J. G., & Korenaga, J. (2012). Terrestrial planet evolution in the stagnant-lid regime: Size effects and the formation of self-destabilizing crust. *Icarus*, *221*(2), 1043–1060. https://doi.org/10.1016/j.icarus.2012.10.015

O'Rourke, J. G., & Stevenson, D. J. (2016). Powering Earth's dynamo with magnesium precipitation from the core. *Nature*, *529*(7586), 387–389. https://doi.org/10.1038/nature16495

O'Rourke, J. G., Gillmann, C., & Tackley, P. (2018). Prospects for an ancient dynamo and modern crustal remanent magnetism on Venus. *Earth and Planetary Science Letters*, *502*, 46–56. https://doi.org/10.1016/j.epsl.2018.08.055

Pozzo, M., Davies, C., Gubbins, D., & Alfè, D. (2012). Thermal and electrical conductivity of iron at Earth's core conditions. *Nature*, *485*(7398), 355–8. https://doi.org/10.1038/nature11031

Rogers, L. A. (2015). Most 1.6 earth-radius planets are not rocky. *Astrophysical Journal*, *801*(1), 41. https://doi.org/10.1088/0004-637X/801/1/41

Scipioni, R., Stixrude, L., & Desjarlais, M. P. (2017). Electrical conductivity of SiO2 at extreme conditions and planetary dynamos. *Proceedings of the National Academy of Sciences of the United States of America*, *114*(34), 9009–9013. https://doi.org/10.1073/pnas.1704762114

Seager, S., Kuchner, M., Hier-Majumder, C. A., & Militzer, B. (2007). Mass-Radius Relationships for Solid Exoplanets. *ApJ*, *669*(2), 1279–1297. https://doi.org/10.1086/521346

Seagle, C. T., Cottrell, E., Fei, Y., Hummer, D. R., & Prakapenka, V. B. (2013). Electrical and thermal transport properties of iron and iron-silicon alloy at high pressure. *Geophysical Research Letters*, *40*(20), 5377–5381. https://doi.org/10.1002/2013GL057930

Smrekar, S. E., Davaille, A., & Sotin, C. (2018). Venus Interior Structure and Dynamics. *Space Science Reviews*, *214*(5), 88. https://doi.org/10.1007/s11214-018-0518-1

Sotin, C., Grasset, O., & Mocquet, A. (2007). Mass-radius curve for extrasolar Earth-like planets and ocean planets. *Icarus*, *191*(1), 337–351. https://doi.org/10.1016/j.icarus.2007.04.006

Soubiran, F., & Militzer, B. (2018). Electrical conductivity and magnetic dynamos in magma oceans of Super-Earths. *Nature Communications*, *9*(1). https://doi.org/10.1038/s41467-018-06432-6

Stamenković, V., Breuer, D., & Spohn, T. (2011). Thermal and transport properties of mantle rock at high pressure: Applications to super-Earths. *Icarus*, *216*(2), 572–596. https://doi.org/10.1016/j.icarus.2011.09.030

Stamenković, V., Noack, L., Breuer, D., & Spohn, T. (2012). the Influence of Pressure-Dependent Viscosity on the Thermal Evolution of Super-Earths. *ApJ*, *748*(1), 41. https://doi.org/10.1088/0004-637X/748/1/41

Stelzer, Z., & Jackson, A. (2013). Extracting scaling laws from numerical dynamo models. *Geophysical Journal International*, *193*(3), 1265–1276. https://doi.org/10.1093/gji/ggt083

Stevenson, D. J. (2003). Planetary magnetic fields. *Earth and Planetary Science Letters*, *208*(1–

2), 1–11. https://doi.org/10.1016/S0012-821X(02)01126-3

Stevenson, D. J. (2010). Planetary magnetic fields: Achievements and prospects. *Space Science Reviews*, *152*(1–4), 651–664. https://doi.org/10.1007/s11214-009-9572-z

Stevenson, D. J., Spohn, T., & Schubert, G. (1983). Magnetism and thermal evolution of the terrestrial planets. *Icarus*, *54*(3), 466–489. https://doi.org/10.1016/0019-1035(83)90241-5

Stixrude, L. (2014). Melting in super-earths. *Philosophical Transactions of the Royal Society A: Mathematical, Physical and Engineering Sciences*, *372*(2014), 20130076. https://doi.org/10.1098/rsta.2013.0076

Stixrude, L., Scipioni, R., & Desjarlais, M. P. (2020). A silicate dynamo in the early Earth. *Nature Communications*, *11*(1), 935. https://doi.org/10.1038/s41467-020-14773-4

Van Summeren, J., Gaidos, E., & Conrad, C. P. (2013). Magnetodynamo lifetimes for rocky, Earth-mass exoplanets with contrasting mantle convection regimes. *Journal of Geophysical Research E: Planets*, *118*(5), 938–951. https://doi.org/10.1002/jgre.20077

Tachinami, C., Senshu, H., & Ida, S. (2011). Thermal evolution and lifetime of intrinsic magnetic fields of super-earths in habitable zones. *Astrophysical Journal*, *726*(2). https://doi.org/10.1088/0004-637X/726/2/70

Tackley, P. J., Ammann, M., Brodholt, J. P., Dobson, D. P., & Valencia, D. (2013). Mantle dynamics in super-Earths: Post-perovskite rheology and self-regulation of viscosity. *Icarus*, *225*(1), 50–61. https://doi.org/10.1016/j.icarus.2013.03.013

Tasker, E., Tan, J., Heng, K., Kane, S., Spiegel, D., Brasser, R., et al. (2017). The language of exoplanet ranking metrics needs to change. *Nature Astronomy*, *1*(February), 1–2. https://doi.org/10.1038/s41550-017-0042

Unterborn, C. T., & Panero, W. R. (2019). The Pressure and Temperature Limits of Likely Rocky Exoplanets. *Journal of Geophysical Research: Planets*, *124*, 1704–1716. https://doi.org/10.1029/2018JE005844

Valencia, D., & O'Connell, R. J. (2009). Convection scaling and subduction on Earth and super-Earths. *Earth and Planetary Science Letters*, *286*(3–4), 492–502. https://doi.org/10.1016/j.epsl.2009.07.015

Valencia, D., O'Connell, R. J., & Sasselov, D. (2006). Internal structure of massive terrestrial planets. *Icarus*, *181*(2), 545–554. https://doi.org/10.1016/j.icarus.2005.11.021

Weiss, L. M., & Marcy, G. W. (2014). The mass-radius relation for 65 exoplanets smaller than 4 earth radii. *Astrophysical Journal Letters*, *783*(1), 1–7. https://doi.org/10.1088/2041-8205/783/1/L6

Wicks, J. K., Smith, R. F., Fratanduono, D. E., Coppari, F., Kraus, R. G., Newman, M. G., et al. (2018). Crystal structure and equation of state of Fe-Si alloys at super-Earth core conditions. *Science Advances*, *4*(4). https://doi.org/10.1126/sciadv.aao5864

Zhang, Y., Hou, M., Driscoll, P., Salke, N. P., Liu, J., Greenberg, E., et al. (2021). Transport properties of Fe-Ni-Si alloys at Earth's core conditions: Insight into the viability of thermal and compositional convection. *Earth and Planetary Science Letters*, *553*, 116614. https://doi.org/10.1016/j.epsl.2020.116614

Ziegler, L. B., & Stegman, D. R. (2013). Implications of a long-lived basal magma ocean in generating Earth's ancient magnetic field. *Geochemistry, Geophysics, Geosystems*, *14*(11), 4735–4742. https://doi.org/10.1002/2013GC005001

AGU PUBLICATIONS

Journal of Geophysical Research: Planets

Supporting Information for

Energetic Requirements for Dynamos in the Metallic Cores of Super-Earth Exoplanets

C. H. Blaske[1,2], J. G. O'Rourke[2]

[1]Barrett, The Honors College, Arizona State University, Tempe AZ

[2]School of Earth and Space Exploration, Arizona State University, Tempe AZ

Contents of this file

Introduction

The supporting information contains one table and four figures that augment the display items in the main text.

M_P (M_E)	k_M (W/m/K)	ρ_M (kg/m^3)	μ_{BL} / $\mu_{BL}(M_E)$	T_{melt} (K)	T_{LM} (K)	$T_C(0)$ (K)	T_{BL} (K)	ΔT_{BL} (K)
1	10	5872	1.00	5000	2635	4089	3362	1454
2	11	6547	1.41	6797	3159	5474	4316	2316
3	13	7110	1.56	8243	3589	6579	5084	2990
4	15	7602	1.64	9480	3981	7528	5755	3547
5	17	8038	1.57	10555	4353	8346	6349	3993
6	20	8441	1.46	11537	4711	9085	6898	4374
7	22	8808	1.4	12423	5060	9765	7412	4705
8	24	9155	1.32	13251	5402	10399	7900	4997
9	26	9481	1.25	14021	5739	10994	8366	5255
10	33	9788	1.22	14743	6070	11560	8815	5490

Table S1. Values of various physical parameters used to calculate the power-law exponents reported in Table 3, including the thermal conductivity of the lower mantle (k_M), the density of the lower mantle (ρ_M), the average viscosity in the thermal boundary layer ratioed to that for an Earth-mass planet ($\mu_{BL}/\mu_{BL}[M_E]$), the melting temperature of silicates in the lower mantle (T_{melt}), the temperature of the lower mantle extrapolated from the potential temperature along an adiabatic gradient (T_{LM}), the temperature at the top of the core when the inner core first nucleates ($T_C[0]$), the average temperature in the boundary layer (T_{BL}) and the thermal contrast across the boundary layer in the lower mantle (ΔT_{BL}). The main text explains how each of these parameters were determined.

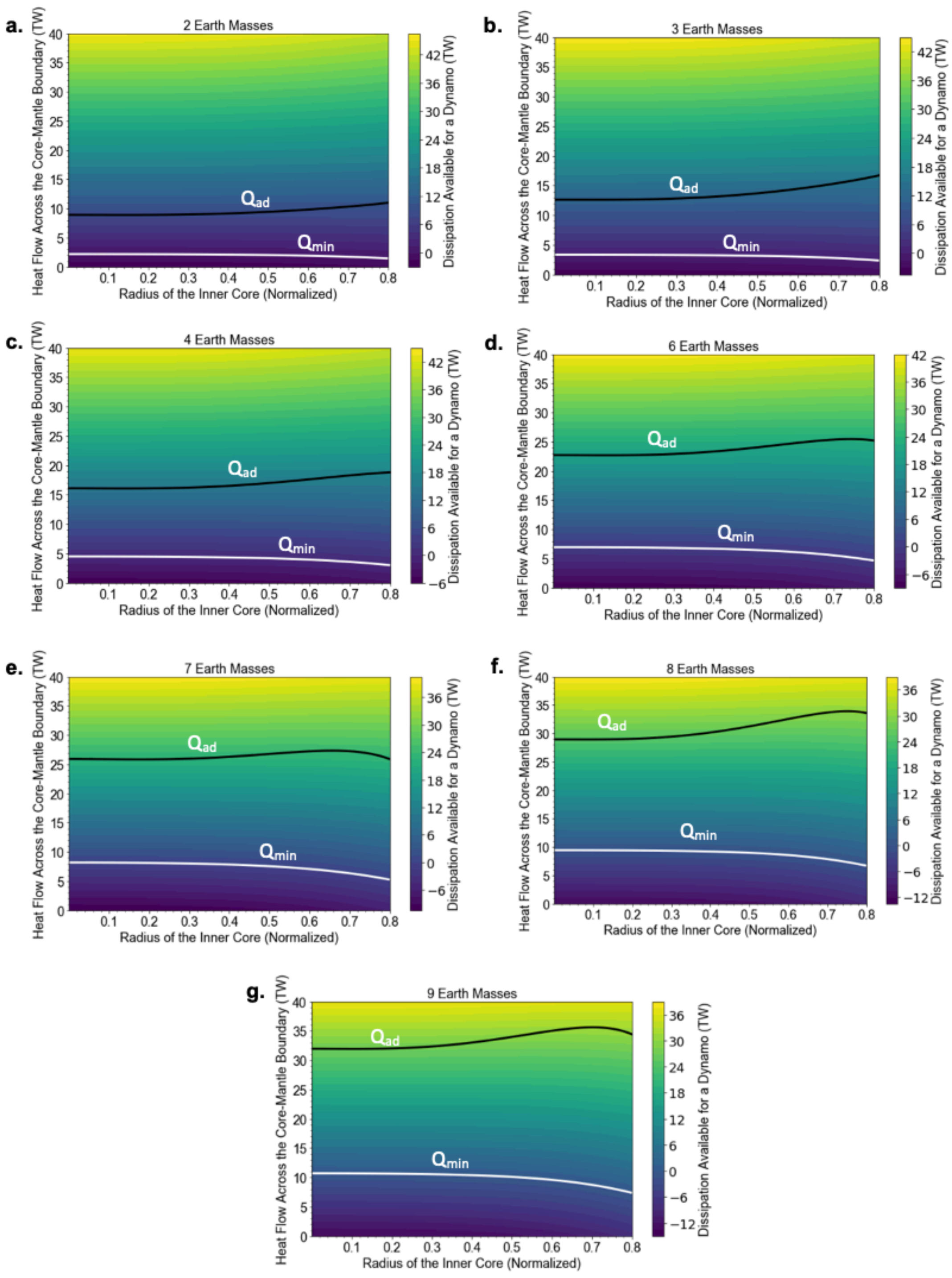

Figure S1. Heat flow required for a dynamo versus the fractional (normalized) radius of the inner core. These subplots are the same as the leftmost column in Figure 3, but for planets with masses that were not included in Figure 3 (e.g., 1–10 M_E in increments of 1 M_E, except 1, 5, and 10 M_E).

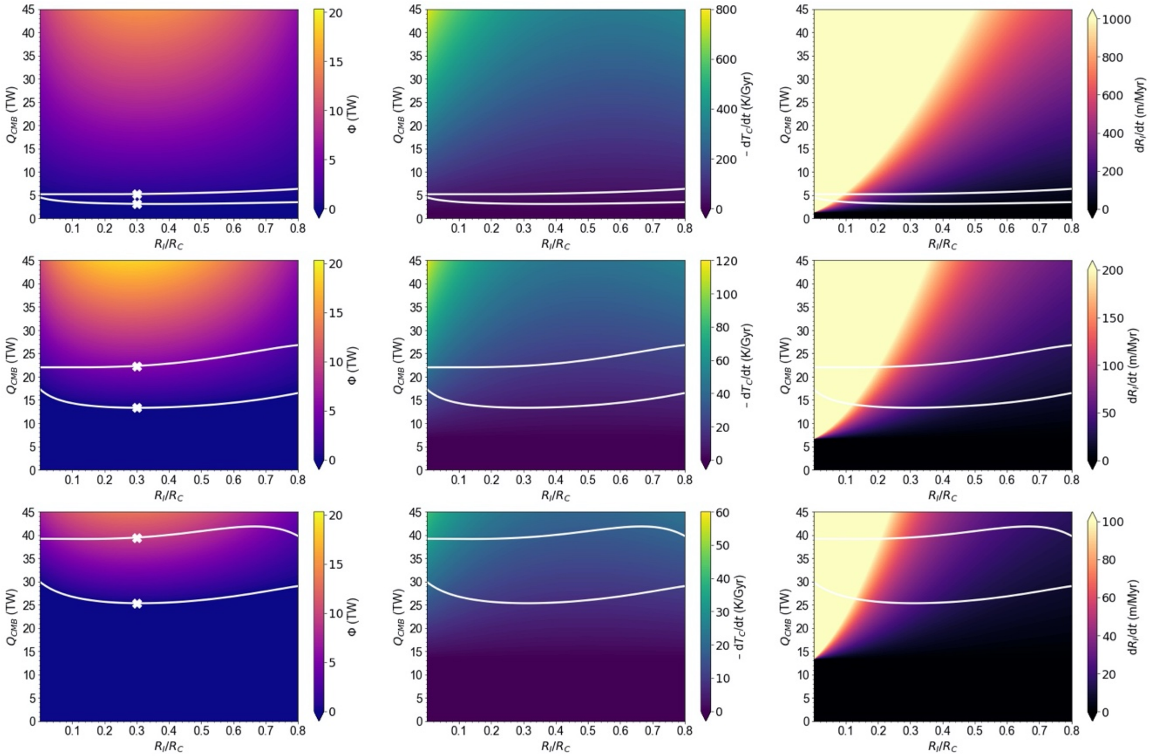

Figure S2. Same as Figure 3, except using the second set of parameters from Table 3 (i.e., [K] = 200 ppm, $P_P = 5 \times 10^{-6}\ \mathrm{K}^{-1}$, and k_C = 40 W/m/K) to explore the effects of radiogenic heating.

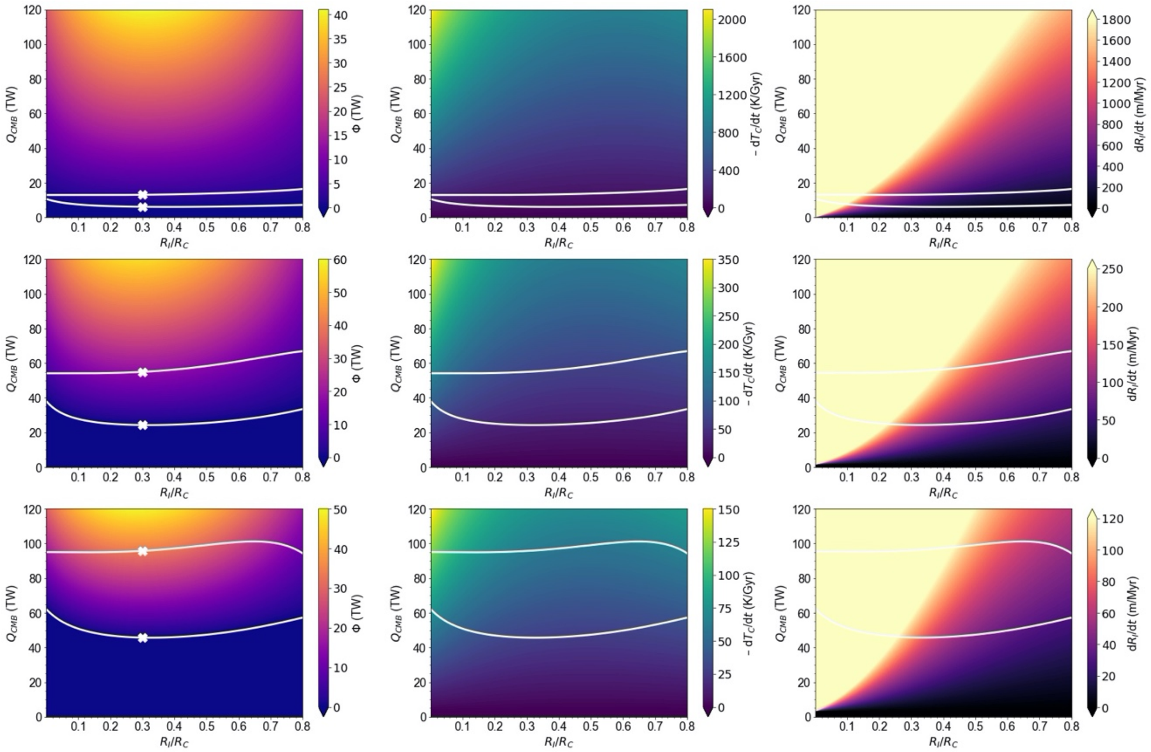

Figure S3. Same as Figure 3, except using the third set of parameters from Table 3 (i.e., [K] = 50 ppm, $P_P = 5 \times 10^{-6}$ K^{-1}, and k_C = 100 W/m/K) to explore the effects of thermal conductivity.

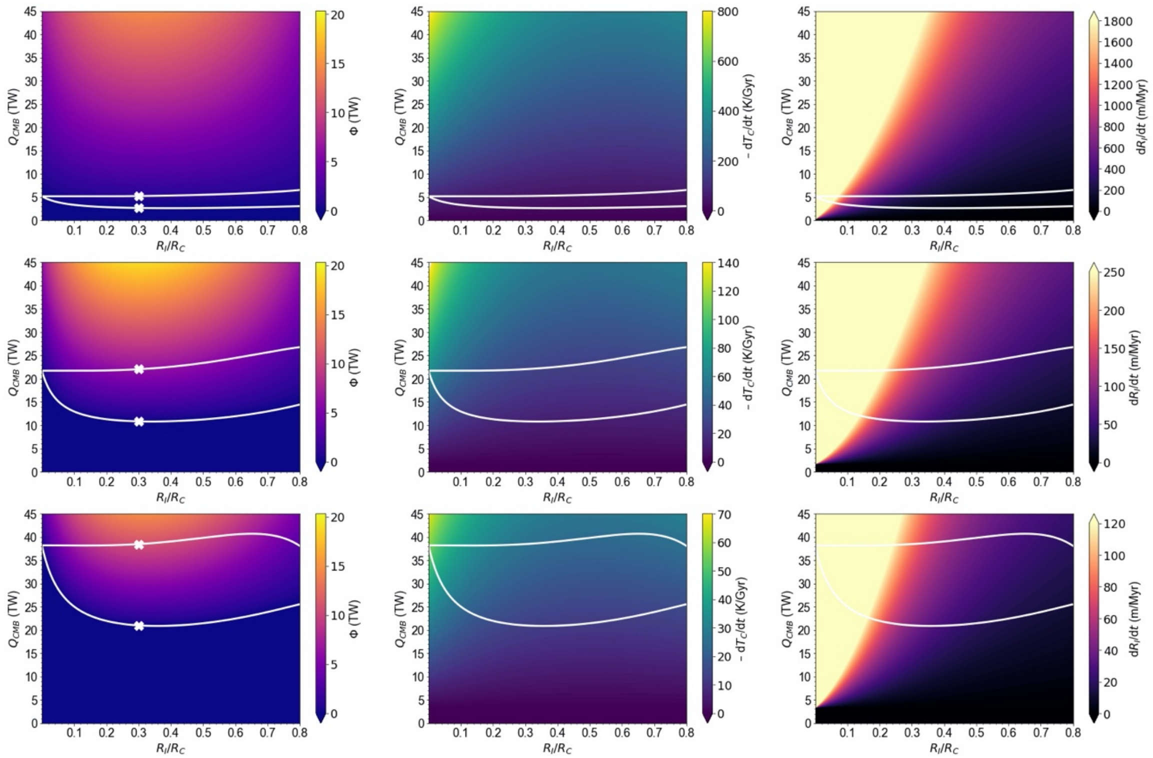

Figure S4. Same as Figure 3, except using the fourth set of parameters from Table 3 (i.e., [K] = 50 ppm, P_P = 0 K^{-1}, and k_C = 40 W/m/K) to explore the effects of the precipitation of light elements from the core at the core-mantle boundary.